Hindawi
Wireless Communications and Mobile Computing
Volume 2021, Article ID 5551674, 7 pages
https://doi.org/10.1155/2021/5551674

Research Article

High-Squint FMCW SAR Imaging via Wavenumber Domain Algorithm

Hui Bi[1], **Hao Li**[1] **and Wei Liang**[2]

[1]*College of Electronic and Information Engineering, Nanjing University of Aeronautics and Astronautics, Nanjing 211106, China*
[2]*Aerospace Information Research Institute, Chinese Academy of Sciences, Beijing 100089, China*

Correspondence should be addressed to Hui Bi; bihui@nuaa.edu.cn

Received 8 January 2021; Revised 14 March 2021; Accepted 22 March 2021; Published 2 April 2021

Academic Editor: Wang Zheng

Nowadays, because the frequency modulation continuous-wave (FMCW) synthetic aperture radar (SAR) shows good potential in minimal transmission power and weight reduction of radar systems, it has been widely used and has become a common technique in modern short-range high-resolution earth observation. Different from the conventional pulsed mode, the stop-to-go approximation is not valid in FMCW SAR. Thus, the typical SAR imaging methods need to be modified to adapt the continuous-wave scheme in practical data processing. In this letter, a wavenumber domain algorithm (WDA) is derived and used for the FMCW SAR imaging under squint and high-squint cases. With the help of the exact scene recovery ability of the proposed WDA, we can achieve the accurate recovery of the considered scene even when using the collected high-squint data and hence obtain the well-focused high-resolution image of the considered scene. Experimental results with simulated and airborne data verify the effectiveness of the proposed method.

1. Introduction

Synthetic aperture radar (SAR) is an active microwave imaging system usually mounted on a satellite or airplane to achieve high-resolution earth observation [1–3]. Compared to typical optical imaging, it has all-time and all-weather surveillance capability and hence has been widely used in early-warning, marine surveillance, and disaster monitoring applications [4]. Compared with a conventional pulse mode-based SAR system, frequency modulation continuous-wave (FMCW) SAR has shown good potential in minimal transmission power and weight reduction of radar systems and hence has been widely used and has become a common technique in modern short-range high-resolution earth observation [5–8]. Different from the typical pulsed imaging mode, FMCW SAR transmits the long sweeps in the data collection process, which will cause the variation of instantaneous slant range and hence makes the stop-to-go approximation not valid any more [5, 9]. To achieve the high-resolution FMCW SAR imaging, in recent years, several algorithms have been proposed and have shown good performance, e.g., range Doppler algorithm (RDA) [10, 11], nonlinear frequency scaling algorithm (FSA) [12], chirp-Z transform-based algorithm [13, 14], and back-projection algorithm (BPA) [15]. Compared with other FMCW SAR imaging methods, because BPA can use the recorded platform position, speed, and posture information effectively, it has shown better performance in SAR image focus from the data with serious trajectory errors. But the huge computational cost of BPA severely restricts its application in practical real-time scene monitoring and early warning. Although RDA and FSA do not need to consider the computational complexity, they have to face the problem caused by the slant range approximation, which will result in the imaging error especially under squint and high-squint cases. In SAR imaging, the two-dimensional (2-D) azimuth-range couple is increased as the squint angle increases, which becomes severe and cannot be ignored in the high-squint case. Therefore, novel algorithms are needed to solve this problem especially in the high-squint FMCW SAR imaging. In 1992, Bamler et al. proposed the wavenumber domain algorithm (WDA) and applied it for pulsed SAR imaging successfully [16, 17]. Because an accurate signal form is used for image focus, WDA has shown the

excellent high-squint data-based high-resolution SAR imaging ability. In 2010, Wang et al. introduced WDA to the side-looking FMCW SAR data processing [9, 18]. With the help of an accurate focus function, WDA has also achieved the high quality scene recovery under the FMCW SAR imaging mode. In this letter, an accurate representation of the WDA algorithm is derived for the FMCW SAR image focusing in squint and high-squint cases. Experimental results show that the proposed method can achieve accurate recovery of the considered scene even when using the collected high-squint data, which means that it can be regarded as a general technique for FMCW SAR imaging in any squint angle. The rest of this letter is organized as follows. Section 2 provides an introduction of the FMCW SAR imaging model with the squint angle. In Section 3, we show the detailed processing procedures of the proposed WDA method for FMCW SAR imaging under squint and high-squint cases. In Section 4, the proposed WDA-based high-squint FMCW SAR method is validated by simulated data to show its advantages in high-resolution image focus. Experimental results via real airborne data as well as a performance analysis are shown in Section 5. Finally, conclusions are drawn in Section 6.

2. FMCW SAR Imaging

In FMCW SAR, let $s(t_r) = \exp\{j2\pi f_0 t_r\} \cdot \exp\{j\pi K_r t_r^2\}$ denote the transmitted signal, where f_0 is the carrier frequency, K_r is the chirp rate of frequency modulated signal, and t_r is the range time. For a single point target $P(\tau_0; r_0)$ with zero Doppler time τ_0 and closest slant range r_0 between $P(\tau_0; r_0)$ and platform trajectory along the line of sight (LOS) direction, we can express the received backscattered energy as

$$g(\tau, t_r, \tau_0; r_0) = \sigma(\tau_0; r_0) \cdot \exp\{j2\pi f_0(t_r - \tau_d)\} \cdot \exp\{j\pi K_r(t_r - \tau_d)^2\}, \tag{1}$$

where τ_d is the round-trip delay time of the wave propagation. Using the reference signal

$$g_{\text{ref}}(t_r) = \exp\{-j2\pi f_0(t_r - \tau_c)\} \cdot \exp\{-j\pi K_r(t_r - \tau_c)^2\}, \tag{2}$$

for the dechirp process in the FMCW SAR system, where r_c is the reference slant range for the dechirp-on-receive operation, and $\tau_c = 2\alpha r_c/c$ with the "Doppler factor" $\alpha = c^2/(c^2 - v^2)$. Then, the received dechirp signal can be expressed as

$$\begin{aligned} g_{\text{de}}(\tau, t_r, \tau_0; r_0) &= g(\tau, t_r, \tau_0; r_0) \cdot g_{\text{ref}}(t_r) \\ &= \sigma(\tau_0; r_0) \exp\{-j2\pi f_0(\tau_d - \tau_c)\} \\ &\quad \cdot \exp\{-j2\pi K_r(\tau_d - \tau_c)(t_r - \tau_c)\} \\ &\quad \cdot \exp\{j\pi K_r(\tau_d - \tau_c)^2\}. \end{aligned} \tag{3}$$

Let $R(\tau)$ denote the instantaneous slant range at time $\tau = t_a + t_r$ with t_a being the azimuth time and θ represent the squint angle. Then, the slant range at the receiver can be expressed as $R(\tau + \tau_d)$, and

$$\tau_d = \frac{R(\tau) + R(\tau + \tau_d)}{c}, \tag{4}$$

with

$$\begin{aligned} R(\tau) &= \sqrt{r_0^2 + v^2(\tau - \tau_0)^2 - 2r_0 v(\tau - \tau_0)\sin\theta}, \\ R(\tau + \tau_d) &= \sqrt{r_0^2 + v^2(\tau + \tau_d - \tau_0)^2 - 2r_0 v(\tau + \tau_d - \tau_0)\sin\theta}, \end{aligned} \tag{5}$$

where v and c are the velocity of the platform and light, respectively. After applying (5) into (4), τ_d has an exact expression, i.e.,

$$\tau_d = 2\alpha\left[\frac{R(\tau)}{c} + \frac{v^2}{c^2}(\tau - \tau_0) - \frac{r_0 v \sin\theta}{c^2}\right]. \tag{6}$$

The last term in (3) is the residual video phase (RVP). After removing the RVP term in the range frequency domain by phase multiplication operation, we have

$$\begin{aligned} g_{\text{de}}(\tau, t_r, \tau_0; r_0) &= \sigma(\tau_0; r_0) \cdot \exp\{-j2\pi f_0(\tau_d - \tau_c)\} \\ &\quad \cdot \exp\{-j2\pi K_r(\tau_d - \tau_c)(t_r - \tau_c)\}. \end{aligned} \tag{7}$$

Using the replacement $f_r = K_r(t_r - \tau_c)$, (7) can be rewritten as

$$g_{\text{de}}(\tau, f_r, \tau_0; r_0) = \sigma(\tau_0; r_0) \cdot \exp\{-j2\pi(f_0 + f_r)(\tau_d - \tau_c)\}. \tag{8}$$

Substituting $\tau = t_a + t_r$ and introducing (6) into (8), we have

$$\begin{aligned} g_{\text{de}}(f_r, t_a, t_r, \tau_0; r_0) &= \sigma(\tau_0; r_0) \cdot \exp\left\{-j4\pi\alpha(f_0 + f_r)\right. \\ &\quad \left. \cdot \left[\frac{R(t_a + t_r)}{c} + \frac{v^2}{c^2}(t_a + t_r - \tau_0) - \frac{r_c}{c} - \frac{r_0 v \sin\theta}{c^2}\right]\right\}. \end{aligned} \tag{9}$$

Then, the Fourier transformation of (9) with respect to t_a is

$$\begin{aligned} G_{\text{de}}(f_a, f_r, t_r, \tau_0; r_0) &= \int g_{\text{de}}(f_r, t_a, t_r, \tau_0; r_0) \\ &\quad \cdot \exp\{-j2\pi f_a t_a\} dt_a \\ &= \sigma(\tau_0; r_0) \int \exp[-j\Phi_1(f_a, f_r, t_a, t_r, \tau_0; r_0)] dt_a, \end{aligned} \tag{10}$$

with

$$\begin{aligned} \Phi_1(f_a, f_r, t_a, t_r, \tau_0; r_0) &= 4\pi\alpha(f_0 + f_r) \\ &\quad \cdot \left[\frac{R(t_a + t_r)}{c} + \frac{v^2}{c^2}(t_a + t_r - \tau_0) - \frac{r_c}{c} - \frac{r_0 v \sin\theta}{c^2}\right] + 2\pi f_a t_a. \end{aligned} \tag{11}$$

To obtain the desired reference spectrum of a point target, by using the principle of stationary phase (POSP), we set the first-order derivative of Φ_1 to be zero to obtain the stationary phase center t_p as

$$t_p = \tau_0 - t_r + \frac{r_0}{v} \cdot h(f_a, f_r), \tag{12}$$

where

$$h(f_a, f_r) = \frac{\sqrt{1 - [cf_a/2\alpha v(f_0 + f_r) + v/c]^2}\sin\theta - [cf_a/2\alpha v(f_0 + f_r) + v/c]\cos\theta}{\sqrt{1 - [cf_a/2\alpha v(f_0 + f_r) + v/c]^2}}. \tag{13}$$

After introducing (12) into (10), we have

$$G_{\mathrm{de}}(f_a, f_r, \tau_0 ; r_0) = \sigma(\tau_0 ; r_0) \cdot \exp\left[-j\Phi(f_a, f_r, \tau_0 ; r_0)\right], \tag{14}$$

with

$$\begin{aligned}\Phi(f_a, f_r, \tau_0 ; r_0) = {} & \frac{4\pi\alpha(f_0 + f_r)r_0}{c} \cdot \left[\sqrt{1 + h(f_a, f_r)^2 - 2h(f_a, f_r)\sin\theta} \right. \\ & \left. + \left[\frac{cf_a}{2\alpha v(f_0 + f_r)} + \frac{v}{c}\right]h(f_a, f_r)\right] - 2\pi f_a \frac{f_r}{K_r} + 2\pi f_a \tau_0 \\ & + 2\pi f_a \tau_0 - 4\pi\alpha(f_0 + f_r)\frac{r_c}{c} - 4\pi\alpha f_a \frac{r_c}{c} - 4\pi\alpha(f_0 + f_r)\frac{r_0 v \sin\theta}{c^2}.\end{aligned} \tag{15}$$

3. WDA-Based Squint and High-Squint Imaging

The procedures of WDA for squint and high-squint FMCW SAR imaging are summarized as follows.

3.1. RVP Removal. In the range frequency domain, a phase multiplication operation is used to remove the RVP term in (3).

3.2. Reference Function Multiplication (RFM). Then, the reference function $G_{\mathrm{ref}}(f_a, f_r ; r_0, r_{\mathrm{ref}}) = exp[j\Phi_{\mathrm{ref}}(f_a, f_r ; r_0, r_{\mathrm{ref}})]$ with

$$\begin{aligned}\Phi_{\mathrm{ref}}(f_a, f_r ; r_0, r_{\mathrm{ref}}) = {} & \frac{4\pi\alpha(f_0 + f_r)r_{\mathrm{ref}}}{c} \\ & \cdot \left[\sqrt{1 + h(f_a, f_r)^2 - 2h(f_a, f_r)\sin\theta} + \left[\frac{cf_a}{2\alpha v(f_0 + f_r)} + \frac{v}{c}\right]h(f_a, f_r)\right] \\ & - 2\pi f_a \frac{f_r}{K_r} 4\pi\alpha(f_0 + f_r)\frac{r_c}{c} - 4\pi\alpha f_a \frac{r_c}{c} - 4\pi\alpha(f_0 + f_r)\frac{r_0 v \sin\theta}{c^2},\end{aligned} \tag{16}$$

is used to remove the range-invariant phase in the 2-D frequency domain. After RFM, the signal becomes

$$\begin{aligned}G_f(f_a, f_r, \tau_0 ; r_0, r_{\mathrm{ref}}) &= G_{\mathrm{de}}(f_a, f_r, \tau_0 ; r_0) \cdot G_{\mathrm{ref}}(f_a, f_r ; r_0, r_{\mathrm{ref}}) \\ &= \sigma(\tau_0 ; r_0) \cdot \exp\left[-j\Phi_{\mathrm{rp}}(f_a, f_r, \tau_0 ; r_0, r_{\mathrm{ref}})\right],\end{aligned} \tag{17}$$

with residual phase

Table 1: Simulation parameters.

Parameter	Value
Radar center frequency	9.6G Hz
Pulse repetition frequency	3200 Hz
Bandwidth	500 MHz
Platform height	1000 m
Down-looking angle	45°

$$\begin{aligned}\Phi_{\mathrm{rp}}(f_a, f_r, \tau_0 ; r_0, r_{\mathrm{ref}}) = {} & \frac{4\pi\alpha(f_0 + f_r)(r_0 - r_{\mathrm{ref}})}{c} \\ & \cdot \left[\sqrt{1 + h(f_a, f_r)^2 - 2h(f_a, f_r)\sin\theta} \right. \\ & \left. + \left[\frac{cf_a}{2\alpha v(f_0 + f_r)} + \frac{v}{c}\right]h(f_a, f_r)\right] - 2\pi f_a \tau_0,\end{aligned} \tag{18}$$

where r_{ref} is the reference slant range. After RFM, the range walk continuous motion is compensated to obtain a coarsely focused image.

3.3. Stolt Interpolation. For $G_f(f_a, f_r, \tau_0 ; r_0, r_{\mathrm{ref}})$, the Stolt interpolation,

$$\begin{aligned}(f_0 + f_r) & \left[\sqrt{1 + h(f_a, f_r)^2 - 2h(f_a, f_r)\sin\theta} \right. \\ & \left. + \left[\frac{cf_a}{2\alpha v(f_0 + f_r)} + \frac{v}{c}\right]h(f_a, f_r)\right] \to f_0 + f_1,\end{aligned} \tag{19}$$

can be achieved by replacing the range frequency f_r with a new one f_1. Then, the signal phase Φ_f in 2-D frequency domain becomes linearly depending on the new range frequency variable f_1, i.e.,

$$\Phi_f(f_a, f_1, \tau_0 ; r_0, r_{\mathrm{ref}}) = \frac{4\pi\alpha(f_0 + f_1)(r_0 - r_{\mathrm{ref}})}{c} - 2\pi f_a \tau_0. \tag{20}$$

3.4. Image Focusing. Finally, we perform 2-D inverse Fourier transform on the signal after Stolt interpolation to obtain the focused image, i.e.,

$$g_f(\tau, t_r, \tau_0 ; r_0, r_{\mathrm{ref}}) = w_a(\tau - \tau_0) \cdot w_r\left(t_r - \frac{2\alpha(r_0 - r_{\mathrm{ref}})}{c}\right), \tag{21}$$

where $w_r(\cdot)$ and $w_a(\cdot)$ are the envelopes in the range and azimuth directions, respectively.

4. Experiment via Simulated Data

In order to validate the derived WDA-based squint and high-squint FMCW SAR imaging method, we first perform the

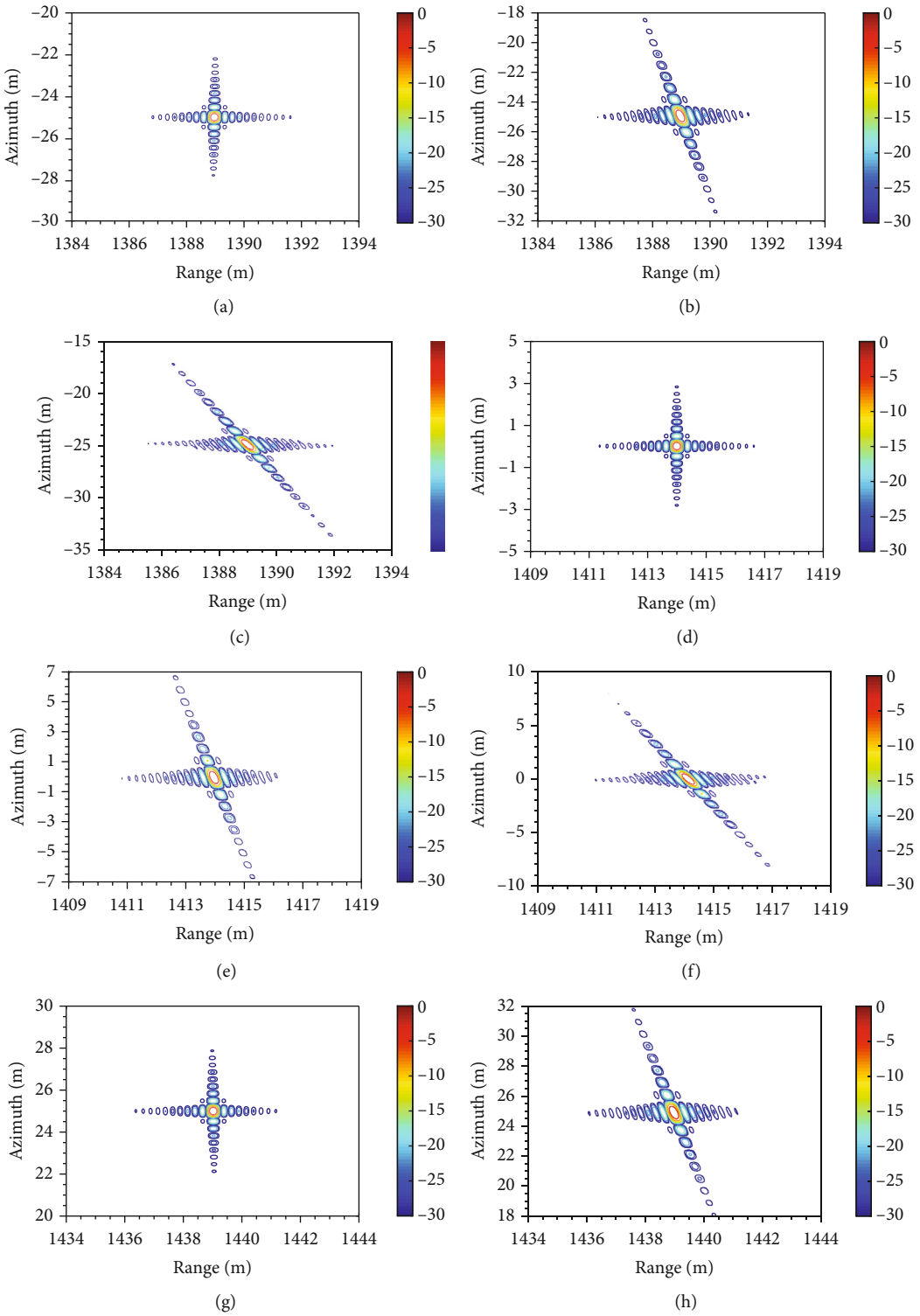

Figure 1: Continued.

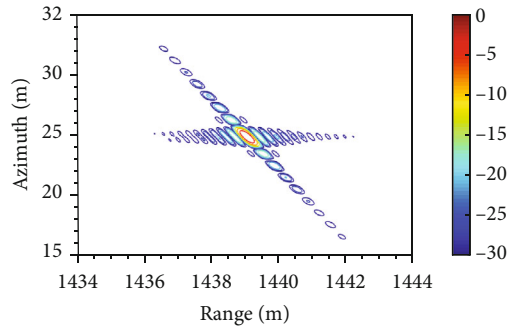

FIGURE 1: Recovered image from the collected data with squint angle $\theta = 0^\circ$ (left column), $\theta = 30^\circ$ (middle column), and $\theta = 45^\circ$ (right column). The targets from top to bottom rows are T1, T2, and T3, respectively.

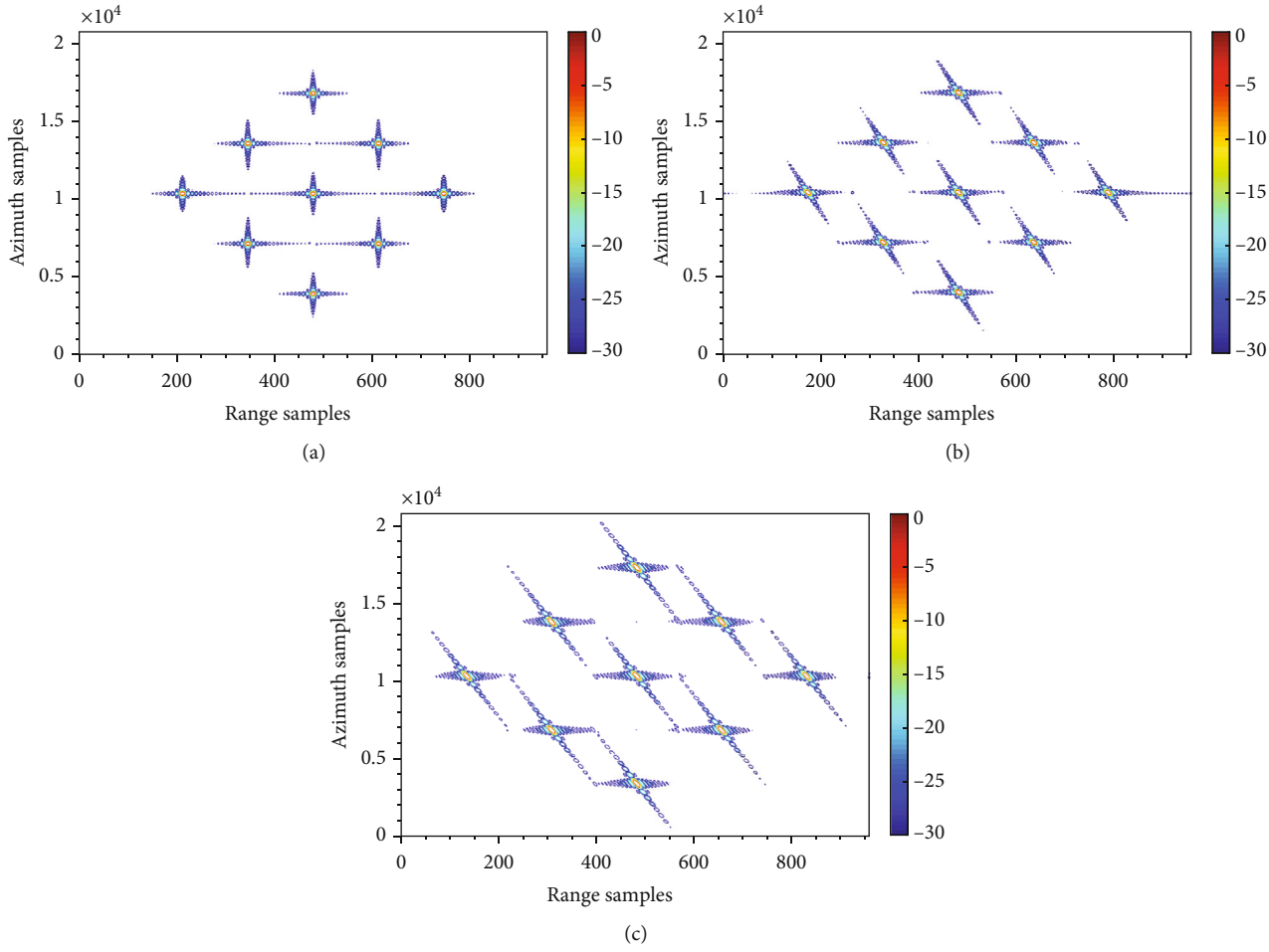

FIGURE 2: Recovered image from the collected data of multitargets with squint angle (a) $\theta = 0^\circ$, (b) $\theta = 30^\circ$, and (c) $\theta = 45^\circ$.

experiment based on the simulated data. The simulated scene includes three point targets, which are located on the near (T1, (R_c −25 m, −25 m)), center (T2, (R_c, 0)), and far ranges (T3, (R_c +25 m, 25 m)). R_c = 1414 m is the center slant range of the considered scene. Simulation parameters are shown in Table 1. Figure 1 shows the WDA-recovered images of three simulated point targets from the collected data with different squint angles. It is seen that when $\theta = 0^\circ$, i.e., the side-looking case, WDA can focus all targets well, which is consistent with the result in [9]. After increasing θ to 30°, we can see that the proposed method can also achieve the accurate recovery of the considered scene. Further increasing the squint angle to 45°, FMCW SAR can be regarded as in the high-squint case. The derived WDA-based method also reconstructs the scene successfully. While for the complicated simulated scene with multitargets, as shown in Figure 2, it is seen that the proposed method also can recover the point targets well even under the high-squint case with a 45° squint angle.

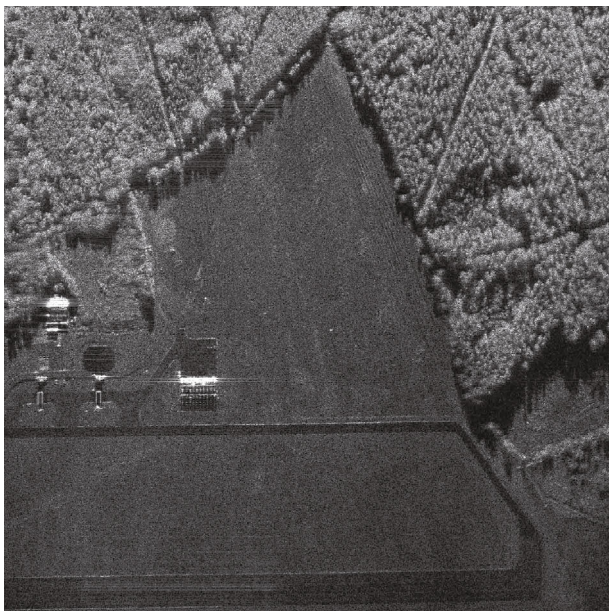

Figure 3: Image of airport area recovered by WDA.

Figure 4: Image of urban area recovered by WDA.

The above experimental results agree with the theoretical analysis, i.e., the derived method achieves the accurate recovery of the considered scene even when using the collected squint and high-squint data. It means that the proposed method in this letter can be regarded as a general technique for both side-looking and squint and high-squint FMCW SAR imaging and can be used further for the practical data processing.

5. Experiment via Real Data

In this section, to further support our viewpoint, the derived method is introduced to the practical airborne FMCW SAR data processing. The WDA-focused images of different surveillance regions are shown in Figures 3 and 4. From Figures 3 and 4, it is seen that WDA can reconstruct the considered scene accurately, such as buildings and the airport runway, which illustrates that the method presented in this letter is effectively used for real FMCW SAR imaging.

6. Conclusion

In this letter, we introduce WDA to FMCW SAR imaging for the cases of squint and high-squint. The exact theoretical derivation of the squint and high-squint FMCW SAR imaging helps us to construct a universal model for WDA-based image focusing, which can make our derived model be used for FMCW SAR imaging from the collected data with any squint angle. Experimental results based on simulated and practical data validate the derived method in image-exact focusing and its potential in real airborne data processing.

Data Availability

No data were used to support this study.

Conflicts of Interest

The authors declare that they have no conflicts of interest.

Acknowledgments

This work was supported by the National Natural Science Foundation of China (61901213), the Natural Science Foundation of Jiangsu Province (BK20190397), the Aeronautical Science Foundation of China (201920052001), the Young Science and Technology Talent Support Project of Jiangsu Science and Technology Association, the Nanjing Science and Technology Innovation Project for Overseas Researcher, the Fundamental Research Funds for the Central Universities (NE2020004), and the Foundation of the Graduate Innovation Center, Nanjing University of Aeronautics and Astronautics (kfjj20200419).

References

[1] J. C. Curlander and R. N. Mcdonough, *Synthetic Aperture Radar: System and Signal Processing*, Wiley, New York, NY, USA, 1991.

[2] F. M. Henderson and A. J. Lewis, *Principle and Application of Imaging Radar*, John Wiley and Sons, New York, NY, USA, 1998.

[3] I. G. Cumming and F. H. Wong, *Digital Processing of Synthetic Aperture Radar Data: Algorithms and Implementation*, Artech House, Norwood, MA, USA, 2004.

[4] H. Bi, B. Zhang, X. X. Zhu, J. Sun, W. Hong, and Y. Wu, "L_1-regularization-based SAR imaging and CFAR detection via complex approximated message passing," *IEEE Transactions on Geoscience and Remote Sensing*, vol. 55, no. 6, pp. 3426–3440, 2017.

[5] H. Bi, J. Wang, and G. Bi, "Wavenumber domain algorithm-based FMCW SAR sparse imaging," *IEEE Transactions on Geoscience and Remote Sensing*, vol. 57, no. 10, pp. 7466–7475, 2019.

[6] A. G. Stove, "Linear FMCW radar techniques," *IEE Proceedings F Radar and Signal Processing*, vol. 139, no. 5, pp. 343–350, 1992.

[7] A. Meta, P. Hoogeboom, and L. P. Ligthart, "Signal processing for FMCW SAR," *IEEE Transactions on Geoscience and Remote Sensing*, vol. 45, no. 11, pp. 3519–3532, 2007.

[8] E. C. Zaugg and D. G. Long, "Theory and application of motion compensation for LFM-CW SAR," *IEEE Transactions on Geoscience and Remote Sensing*, vol. 46, no. 10, pp. 2990–2998, 2008.

[9] R. Wang, O. Loffeld, H. Nies, S. Knedlik, M. Hagelen, and H. Essen, "Focus FMCW SAR data using the wavenumber domain algorithm," *IEEE Transactions on Geoscience and Remote Sensing*, vol. 48, no. 4, pp. 2109–2118, 2010.

[10] M. De Wit, A. Meta, and P. Hoogeboom, "Modified range-Doppler processing for FM-CW synthetic aperture radar," *IEEE Geoscience and Remote Sensing Letters*, vol. 3, no. 1, pp. 83–87, 2006.

[11] G. Jia, M. Buchroithner, W. Chang, and X. Li, "Simplified real-time imaging flow for high-resolution FMCW SAR," *IEEE Geoscience and Remote Sensing Letters*, vol. 12, no. 5, pp. 973–977, 2015.

[12] A. Meta, P. Hoogeboom, and L. P. Ligthart, "Non-linear frequency scaling algorithm for FMCW SAR data," in *2006 European Radar Conference*, pp. 9–12, Manchester, UK, Septemebr 2006.

[13] Y. Liu, Y. Deng, and R. Wang, "Focus squint FMCW SAR data using inverse chirp-*Z* transform based on an analytical point target reference spectrum," *IEEE Geoscience and Remote Sensing Letters*, vol. 9, no. 5, pp. 866–870, 2012.

[14] D. Li, H. Lin, H. Liu, H. Wu, and X. Tan, "Focus improvement for squint FMCW-SAR data using modified inverse chirp-*Z* transform based on spatial-variant linear range cell migration correction and series inversion," *IEEE Sensors Journal*, vol. 16, no. 8, pp. 2564–2574, 2007.

[15] A. Ribalta, "Time-domain reconstruction algorithms for FMCW-SAR," *IEEE Geoscience and Remote Sensing Letters*, vol. 8, no. 3, pp. 396–400, 2011.

[16] R. Bamler, "A comparison of range-Doppler and wavenumber domain SAR focusing algorithms," *IEEE Transactions on Geoscience and Remote Sensing*, vol. 30, no. 4, pp. 706–713, 1992.

[17] H. J. Callow, M. P. Hayes, and P. T. Gough, "Wavenumber domain reconstruction of SAR/SAS imagery using single transmitter and multiple-receiver geometry," *Electronics Letters*, vol. 38, no. 7, pp. 336–338, 2002.

[18] R. Wang, Y. Luo, Y. Deng, Z. Zhang, and Y. Liu, "Motion compensation for high-resolution automobile FMCW SAR," *IEEE Geoscience and Remote Sensing Letters*, vol. 10, no. 5, pp. 1157–1161, 2013.